



CHALMERS

Chalmers Publication Library

Sulfur Tolerance of $\text{Ca}_x\text{Mn}_{1-y}\text{MyO}_3$ (M = Mg, Ti) Perovskite-Type Oxygen Carriers in Chemical-Looping with Oxygen Uncoupling (CLOU)

This document has been downloaded from Chalmers Publication Library (CPL). It is the author's version of a work that was accepted for publication in:

Energy & Fuels (ISSN: 0887-0624)

Citation for the published paper:

Arjmand, M. ; Kooiman, R. ; Rydén, M. (2014) "Sulfur Tolerance of $\text{Ca}_x\text{Mn}_{1-y}\text{MyO}_3$ (M = Mg, Ti) Perovskite-Type Oxygen Carriers in Chemical-Looping with Oxygen Uncoupling (CLOU)". *Energy & Fuels*, vol. 28(2), pp. 1312â1324.

<http://dx.doi.org/10.1021/ef402383v>

Downloaded from: <http://publications.lib.chalmers.se/publication/193522>

Notice: Changes introduced as a result of publishing processes such as copy-editing and formatting may not be reflected in this document. For a definitive version of this work, please refer to the published source. Please note that access to the published version might require a subscription.

Chalmers Publication Library (CPL) offers the possibility of retrieving research publications produced at Chalmers University of Technology. It covers all types of publications: articles, dissertations, licentiate theses, masters theses, conference papers, reports etc. Since 2006 it is the official tool for Chalmers official publication statistics. To ensure that Chalmers research results are disseminated as widely as possible, an Open Access Policy has been adopted. The CPL service is administrated and maintained by Chalmers Library.

(article starts on next page)

Sulphur Tolerance of $\text{Ca}_x\text{Mn}_{1-y}\text{M}_y\text{O}_{3-\delta}$ (M = Mg, Ti) Perovskite-type Oxygen Carriers in Chemical-Looping with Oxygen Uncoupling (CLOU)

Mehdi Arjmand^{a,*}, *Roeland F. Kooiman*^b, *Magnus Rydén*^c, *Henrik Leion*^a, *Tobias Mattisson*^c, *Anders Lyngfelt*^c

^a Department of Chemical and Biological Engineering, Division of Environmental Inorganic Chemistry, Chalmers University of Technology, SE-412 96 Göteborg, Sweden

^b Department of Chemical Engineering and Chemistry, Eindhoven University of Technology, NL-5600MB, Eindhoven, the Netherlands

^c Department of Energy and Environment, Division of Energy Technology, Chalmers University of Technology, SE-412 96 Göteborg, Sweden

* To whom correspondence should be addressed. Telephone: +46-31-772-2822;

Abstract

Perovskite-structured oxygen carriers of the type $\text{Ca}_x\text{Mn}_{1-y}\text{M}_y\text{O}_{3-\delta}$ ($\text{M} = \text{Mg}, \text{Ti}$) have been investigated for the CLOU process. The oxygen carrier particles were produced by spray drying and were calcined at 1300°C for 4 h. A batch fluidized-bed reactor was used to investigate the chemical-looping characteristics of the materials. The effect of calcium content, dopants (Mg and Ti) and operating temperature (900, 950, 1000 and 1050°C) on the oxygen uncoupling property and the reactivity with CH_4 in presence and absence of SO_2 was evaluated. In addition, the attrition resistance and mechanical integrity of the oxygen carriers were examined in a jet-cup attrition rig. All of the investigated perovskite-type materials were able to release gas phase oxygen in inert atmosphere. Their reactivity with methane was high and increased with temperature and calcium content, approaching complete gas yield at 1000°C . The reactivity decreased in the presence of SO_2 for all of the investigated oxygen carriers. Decreasing the calcium content resulted in a less severe decrease in reactivity in the presence of SO_2 , with the exception of materials doped with both Mg and Ti, for which a higher resistance to sulphur deactivation could be maintained even at higher calcium contents. The drop in reactivity in the presence of SO_2 also decreased at higher temperatures and at 1050°C , the decrease in the reactivity of the Mg- and Ti-doped material was minimal. Sulphur balance over the reactor system indicated that the fraction of the introduced SO_2 that passed through the reactor increased with temperature. It was shown that it is possible to regenerate the oxygen carriers during reduction in the absence of SO_2 . Most of the materials also showed relatively low attrition rates. The results indicate that it is possible to modify the operating conditions and properties of perovskite-type oxygen carriers to decrease or avoid their deactivation by sulphur.

Keywords: CO_2 -capture; chemical-looping combustion (CLC); chemical-looping with oxygen uncoupling (CLOU); oxygen carrier; perovskite-structured, sulphur deactivation.

1. Introduction

The chemical-looping combustion (CLC) and chemical-looping with oxygen uncoupling (CLOU) are innovative processes for efficient combustion of hydrocarbon fuels with inherent separation of carbon dioxide.¹⁻³ Chemical-looping has the great advantage of capturing CO₂ without the energy and cost penalties resulting from gas separation, which cannot be avoided in other CO₂ capture technologies.^{2, 4, 5} Until now, CLC has been successfully demonstrated in a number of units of sizes up to 120 kW⁶ and reviews of current achievements in CLC are given by Lyngfelt,⁶⁻⁸ Hossain and de Lasa⁹, Adanez et al.¹⁰ and Fan et al.¹¹

In the fuel reactor of a chemical-looping system, a gas-solid reaction is preferred over a solid-solid reaction due to the much faster reaction rates. This is particularly important with respect to applications for solid fuels, which means that solid fuels must be gasified initially with steam or CO₂ to produce CO and H₂ gases which can then react with the solid oxygen carrier material.¹²⁻¹⁶ Since the gasification of a solid fuel is a rather slow process, the gasification step in CLC becomes the rate-determining step in the overall process. Therefore, another technique can be used for solid fuels which is called chemical-looping with oxygen uncoupling (CLOU).¹⁷ In CLOU, the oxygen carrier releases gaseous oxygen which can then react directly with the solid fuel as in normal combustion. For this reason, the gasification process can be avoided in CLOU. The source of the gaseous oxygen in CLOU is the oxygen carrier material. Demonstration of the CLOU process¹⁸ has proven the advantage of this technology over the CLC process, where slow gasification is an imperative step.¹⁹ Moreover, the solids inventory in the fuel reactor of the CLOU process would be lower than in CLC due to faster fuel conversion,²⁰ thus limiting the need for a carbon stripper or additional treatments. In CLOU, thermodynamic equilibrium governs the uncoupling of gaseous oxygen from the oxygen carrier and the subsequent oxidation of the reduced oxygen carrier to its initial state in the air reactor. Therefore, a required property for the oxygen carrier in CLOU is that it must be able to both react with O₂ (oxidize) and release O₂ at temperatures suitable for the process, i.e. 800 to 1200°C.

The CuO–Cu₂O oxide pair is one of the prominent monometallic oxygen carriers suitable for the CLOU process, along with Mn₂O₃–Mn₃O₄ and CoO–Co₃O₄ oxide pairs.²¹⁻²³ For pure Mn₂O₃–Mn₃O₄, reoxidation is restricted to lower temperatures (below 800°C), which are of less practical importance for a realistic CLC unit. It is however possible to overcome this thermodynamic constraint by combining manganese oxide with other oxides, for instance Ni, Cu, Si, Mg, Si, Fe.²¹⁻²³ Co-based oxygen carriers are however, less attractive due to cost,

health and environmental issues. A third group of manufactured oxygen carriers suitable for the CLOU process are ABO_3 perovskite-type materials.²⁴⁻³⁴ These materials can release a significant amount of oxygen through,



Here δ is the degree of oxygen non-stoichiometry in the perovskite-structured material and AR and FR refer to the value of δ in the air and the fuel reactor, respectively. The amount of oxygen that can be released or taken up depends on the oxygen partial pressure and the temperature in the fuel and the air reactors. The A- and the B-sites can also be doped or substituted with other elements, and thus a number of different perovskites can be synthesized. One promising group of perovskite-type oxygen carrier materials belongs to the calcium manganate ($CaMnO_{3-\delta}$) family and its slightly altered variants, which have shown excellent behaviour for gaseous fuel combustion in continuous operation.^{35, 36} It has also been reported that doping at the A- and/or B-sites can significantly affect the oxygen-carrying capacity, performance, reactivity and stability of the oxygen carrier.²⁴

Using perovskite-type oxygen carriers in CLC or CLOU is not without limitations. Sulphur is present in significant concentrations in solid fuels and to a lesser extent in natural gas. Several studies have investigated the use of perovskite-structured materials in fuel cell applications and have found that these oxides can be highly susceptible to deactivation in the presence of sulphur-containing compounds.³⁷⁻⁴² The general consensus is that the deactivation of these materials by SO_2 or H_2S occurs in two steps. Initially, the sulphur-containing species binds or adsorbs to certain active sites by pairing with oxygen ion vacancies. Then, the adsorbed sulphur species is converted to sulphite (e.g. $CaSO_3$ or $LaSO_3$) and after that to a sulphate species (e.g. $CaSO_4$ or $LaSO_4$).⁴³ Severe deactivation of perovskite-type materials have been reported after exposure to even small amounts of SO_2 which has been ascribed to phase separation and the formation of sulphates.³⁹⁻⁴² Substitution with transition metal elements such as Ti, Zr, V, Sn, Cu or Cr might make the SO_2 bonding with the surface weaker, and therefore could result in higher resistance to SO_2 poisoning.^{43, 44} For instance, the presence of Mn at the B site increases the reactivity for methane conversion but makes such materials more prone to poisoning by SO_2 , while the presence of Cr at the B site decreases the former and increases the latter, owing to the acidic nature of Cr.³⁸ Moreover, the addition of MgO to such materials could slow the deactivation process, as MgO preferentially reacts with sulphur, thus allowing the perovskite-structured material to avoid deactivation for a longer period of

time.⁴⁵ It should be mentioned however, that operating conditions such as oxygen partial pressures and/or temperatures in CLC or CLOU are substantially different from those encountered in fuel cell applications, which necessitates additional research on this matter.

Predicting the behaviour of $\text{CaMnO}_{3-\delta}$ during the chemical-looping combustion of sulphur-containing fuels is not a trivial task. Earlier studies on the use of limestone (CaCO_3) in fluidized-bed combustion (FBC) for capturing SO_2 provide some information on the possible reaction pathways in the system Ca-S-O under oxidizing and reducing conditions,⁴⁶⁻⁴⁸ which are summarized in Table 1. It is possible to envisage the occurrence of similar reactions in the fuel and the air reactor of a CLC or CLOU unit for perovskite-type oxygen carriers should calcium in a perovskite-structured material form CaSO_4 or CaS . Of particular importance in Table 1 are the decomposition reactions of CaSO_4 under reducing conditions, i.e. equations (5)–(7), which indicate that CaSO_4 is not stable under reducing conditions.

Figure 1 shows the stability regions of CaS , CaO and CaSO_4 as a function of temperature and partial pressure of O_2 and SO_2 using FactSage[®] 6.3.1.⁴⁹ It can be readily seen that CaO is thermodynamically more stable than CaSO_4 and CaS at certain partial pressures of O_2 and SO_2 . Worth noting is that the stable region for CaO increases with temperature, thus favouring the decomposition of CaSO_4 or CaS .

Figure 1 would be slightly different if $\text{CaMnO}_{3-\delta}$ was replaced with CaO . While precise thermodynamic data on the $\text{CaMnO}_{3-\delta}$ perovskite-structured materials is lacking, it is helpful to consider $\text{CaMnO}_{3-\delta}$ as being composed of the two individual components CaO and $\text{MnO}_{2-\delta}$. It is known that a mixture of calcium and manganese oxides of the correct stoichiometry spontaneously forms perovskite-type materials during calcination, at least above 1000°C . This indicates that $\text{CaMnO}_{3-\delta}$ is more strongly favoured thermodynamically at these temperatures than calcium and manganese oxides. Considering that manganese oxides are inert to sulphur species at these temperatures, it is expected that the window of operation without the formation of solid sulphur compounds should be larger for $\text{CaMnO}_{3-\delta}$ than for CaO .

Research on the tolerance of perovskite-type oxygen carriers to sulphur deactivation in CLC or CLOU is very limited. Reactivity testing with $\text{CaMn}_{0.875}\text{Ti}_{0.125}\text{O}_{3-\delta}$ as oxygen carrier using CH_4 at 950°C in the presence of SO_2 has suggested a decrease in reactivity, most likely due to the formation of CaSO_4 .⁵⁰ The aim of this study is to investigate the sulphur tolerance of different calcium-manganese-based oxygen carriers in CLOU. The effect of the calcium content, dopants (Mg and Ti) and the effect of operating temperature (900 , 950 , 1000 and 1050°C) on the oxygen uncoupling property and the reactivity of oxygen carriers with

methane has been evaluated. In addition, the mechanical and attrition resistance of the oxygen carriers has been evaluated in a jet-cup attrition rig. To investigate the influence of sulphur on reactivity of oxygen carriers and their oxygen release ability, the oxygen carrier particles have been exposed to SO₂ during reduction, to simulate the sulphur that would be released from sulphur-containing solid fuels. Using an overall mass balance over the reactor system for sulphur, it has been possible to evaluate the sulphur tolerance and the degree of sulphur deactivation of the investigated materials.

2. Experimental

2.1 Preparation and fabrication of the oxygen carriers

The oxygen carriers prepared in this investigation are summarized in Table 2. The particles were manufactured by spray-drying at VITO (Flemish Institute for Technological Research, Belgium) using the intended combination of Mn₃O₄ (Trimanox, Chemalloy), Ca(OH)₂ (Nordkalk), MgO (MagChem 30, Martin Marietta Magnesia Specialties) and TiO₂ (Alfa Aesar). Details of the spray drying technique can be found elsewhere.^{32, 51} The spray-dried particles were calcined at 1300°C for 4 h and were then sieved through stainless steel screens to yield particles in the range of 125–180 and 180–250 μm.

2.2 Characterization of the oxygen carriers

The crystalline phases of the oxygen carriers were identified using powder X-ray diffraction (Bruker AXS, D8 Advanced) with CuK_{α1} radiation. The bulk (tapped) density was obtained for particles in the size range of 125–180 μm with a graduated cylinder and a scale. The Brunauer-Emmett-Teller (BET) specific surface area was determined using N₂-adsorption (Micromeritics, TriStar 3000). The crushing strength, i.e. the force needed to fracture a single particle, was measured by using a digital force gauge (Shimpo, FGN-5) for particles in the size range of 180–250 μm. 30 measurements were made of each sample and the average value was chosen as the representative crushing strength. The morphology of the particles was examined with an environmental scanning electron microscope (ESEM) fitted with a field emission gun (FEI, Quanta 200) and energy-dispersive X-ray (EDX).

In order to assess the oxygen capacity (R_O) of the investigated materials for CLOU, a thermogravimetric analyser (Netzsch, STA 409 PC *Luxx*) was used. Approximately 20 mg of a used sample (125–180 μm) from the reactivity experiment in the fluidized-bed reactor following oxidation in 5% O₂ was used. The sample was exposed to high purity N₂ with an inlet flow rate of 20 mL_N/min. The heating rate was a linear ramp of 40°C/min and after

reaching 1000°C, the temperature was maintained constant for 30 min. Prior to this, the thermobalance was calibrated with an empty Al₂O₃ crucible under identical experimental conditions.

The attrition rate of the particles sized 125–180 µm was measured using a customized jet-cup attrition rig,⁵² which simulates the effects of grid jet attrition and cyclone attrition in a circulating fluidized-bed combustor, details of which can be found elsewhere.^{24, 51}

2.3 Experimental setup and procedure in the fluidized-bed reactor

A laboratory-scale fluidized-bed reactor system was used for examining the oxygen uncoupling behaviour and the reactivity of the oxygen carriers. A more detailed description of the reactor system has been presented previously.^{24, 51, 53, 54} In order to obtain an understanding of the degree of deactivation of perovskite-structured oxygen carriers, a mass balance for sulphur must be made over the reactor system. However, a major difficulty arose due to the high solubility of SO₂ in water⁵⁵ resulting in the partial loss of SO₂ in the condensed water produced from the conversion of methane during reduction. In the previously used experimental setups,^{24, 53, 54} the exit gas stream from the reactor was led into a condenser to remove the water formed during the conversion of methane. In the present study, the condenser was replaced with a filter pipe directly after the sampling probe, followed by a short heated line. The filter was filled with granulated magnesium perchlorate anhydrous (Mg(ClO₄)₂) as the drying agent in order to dry the effluent stream. Thus, SO₂ was prevented from dissolving in the water produced during the conversion of methane.

A summary of the experimental procedure is outlined in Table 3. Initially, the reactivity and the oxygen release ability of the materials were investigated. Here, 15 g of the sample sized 125–180 µm was placed on the porous plate and the reactor was heated to 900°C in 5% O₂-balance N₂ mixture in order to fully oxidize the oxygen carrier. The rationale for using 5% O₂ was to determine whether the oxygen carrier could be oxidized in conditions similar to those at the outlet of the air reactor in a realistic CLC unit. Hereinafter, the term ‘cycle’ will be used to describe a sequence of reduction-oxidation periods. The reducing periods consisted of exposures to either an inert (N₂) or a fuel (CH₄) gas, followed by oxidation with the aforementioned 5% O₂ mixture. Fuel cycles with 50% CH₄-balance N₂ for 20 s during the reduction period were conducted at the temperatures 900, 950 and 1000°C. Nitrogen was used as an inert purge gas for 60 s in between oxidation and reduction periods to avoid gases being mixed during the preceding reduction or the succeeding oxidation period. After the fuel

cycles, inert (N₂) gas cycles were conducted at 900, 950 and 1000°C for 360 s, to investigate the oxygen release ability.

In order to investigate the tolerance of the oxygen carrier towards sulphur deactivation, the stream of 50% CH₄–balance N₂ used in the reduction phase was substituted with a stream of 50% CH₄–0.5% SO₂–balance N₂. Thus, the concentration of SO₂ in this stream corresponds to 5000 vppm which is representative of a low-sulphur coal. The fuel cycles were carried out in a similar way followed by inert (N₂) gas cycles, with the difference that the order of the experimental temperatures was 1000, 950 and 900°C. This was to minimize the deactivation process of the oxygen carriers by virtue of lower favourability of CaSO₄ formation at higher temperatures, as shown in Figure 1.

To establish reproducibility of the results, all inert gas (N₂) cycles and fuel cycles in the absence of SO₂ were repeated three times, while fuel cycles in the presence of SO₂ were repeated five times. Thus, the performance of each oxygen carrier was evaluated for a total of 42 fuel and inert cycles. The flow rate was kept constant at 900 mL_N/min during reduction, inert and oxidation periods. This flow rate corresponded to a superficial gas velocity, U , in the reactor of approximately 9 to 21 and 12 to 26 times higher than the calculated minimum fluidization gas velocity, U_{mf} , of the oxygen carrier particles during reduction (with 50% CH₄) and inert (N₂) and oxidation periods (5% O₂), respectively. The minimum fluidization velocity, U_{mf} , was calculated using the correlation given by Kunii and Levenspiel.⁵⁶ However, it should be noted that due to gas expansion during reduction, the actual velocity in the bed was higher, as one mole of CH₄ can be converted to one mole of CO₂ and two moles of H₂O.

2.4 Data analysis

When methane was used as the fuel, it was converted to CO, H₂, H₂O and CO₂ during the reduction period. The reactivity of a given oxygen carrier was quantified in terms of gas yield or conversion efficiency, γ , and was defined as the volume fraction, y_i , of fully oxidized fuel, CO₂, divided by the sum of all the volume fractions of carbon containing gases, i.e. CH₄, CO and CO₂, in the outlet stream,

$$\gamma_{CH_4} = \frac{y_{CO_2}}{y_{CO_2} + y_{CH_4} + y_{CO}} \quad (2)$$

Here, y_i denotes the concentration (vol.%) of each respective gas measured with the gas analyser.

The oxygen carrying capacity, R_O , of the investigated carriers for CLOU is defined as the mass change of oxygen in the samples as follows:

$$R_O = \frac{m_{ox} - m_{red}}{m_{ox}} \quad (3)$$

where m_{ox} and m_{red} are the mass of the oxygen carrier in oxidized and reduced states, respectively.

The mass-based conversion of the oxygen carrier ω is defined as.

$$\omega = \frac{m}{m_{ox}} \quad (4)$$

where m is the actual mass of the oxygen carrier in the reactor. Since it is not possible to measure the mass of the oxygen carrier in the reactor while cycling between different phases, a mass balance for oxygen has been made over the reactor system. Consequently, by measuring the concentrations of various gaseous species in the gas analyser, the mass-based conversion ω of the oxygen carrier can be calculated via

$$\omega_i = 1 - \int_{t_0}^{t_1} \frac{\dot{n}_{out} M_O}{m_{ox}} (4y_{CO_2} + 3y_{CO} + 2y_{O_2} - y_{H_2}) dt \quad (5)$$

where ω_i is the instantaneous mass-based conversion at time t_1 , \dot{n}_{out} is the molar flow rate of dry gas at the reactor outlet as measured by the analyser, M_O is the molar mass of oxygen and t_0 and t_1 are the initial and final times of measurement.

In order to facilitate a comparison between different oxygen carriers at varying temperatures, $\gamma_{CH_4,ave}$, has been used defined as the average of gas yield in Eq. (5) for the period of ω from 1 to 0.99.

The total SO_2 yield, η_{SO_2} , due to the adsorption of sulphur and/or reaction with the oxygen carrier particles has been determined using a mass balance for SO_2 over the reactor system via,

$$\eta_{SO_2} = \frac{n_{SO_2,out}}{n_{SO_2,in}} \quad (6)$$

where $n_{SO_2,in}$ are the moles of SO_2 introduced to the reactor and $n_{SO_2,out}$ are the moles of SO_2 in the effluent during the entire cycle. Thus, $\eta_{SO_2} = 1$ indicates that all SO_2 has passed through the reactor and is seen by the gas analyser, while $\eta_{SO_2} = 0$ implies that all SO_2 has been absorbed by and/or reacted with the oxygen carrier particles.

3. Results and Discussion

3.1 Oxygen uncoupling of the oxygen carriers

The oxygen uncoupling profile during an inert gas period is shown as an example in Figure 2 for C46MTMg at 900, 950 and 1000°C. An inert period at 900°C for sand particles has been included in this figure for comparison. Similar to C46MTMg, all investigated materials released a substantial amount of oxygen. In this particular case, the oxygen release increased with temperature. The oxygen released decreased steadily as a function of time due to the oxygen non-stoichiometry, δ , being dependent on the defect chemistry and oxygen partial pressure in the ambient, according to Eq. (1), which is typical for perovskite-type materials.^{24, 29, 32, 33} There was little difference in the oxygen release profiles during cycling, indicating a stable oxygen uncoupling property for all materials.

To facilitate the comparison of the oxygen uncoupling property among the different investigated perovskite-type materials prior to and after fuel cycles in the presence and absence of SO₂, an average oxygen concentration during the inert phase has been used in Figure 3. In order to avoid any influence on the results from the oxygen remaining in the reactor from the oxidation phase, the average oxygen concentration has been calculated for the inert phase starting from 100 s into the inert period and until the end of the period. The ten perovskite-type oxygen carriers have been categorized into three different groups, namely undoped, doped with Mg and doped with Mg and Ti, all three groups contained materials with different calcium content. It can be observed in Figure 2 that all of the investigated perovskite-structured materials were able to release oxygen and therefore have CLOU ability. During inert periods following the fuel cycles in the absence of SO₂, the undoped and the Mg-doped materials showed the same trend of an increase in the average oxygen concentration with a rise in the temperature from 900 to 950°C. However, for both of these materials, the average oxygen concentration at 1000°C fell below that at 900°C, suggesting that it was not possible to fully oxidize these materials at 1000°C. The materials doped with both Mg and Ti showed an increase in the average oxygen concentration with a rise in temperature from 900 to 1000°C.

It can also be seen that, in general, lowering the calcium content in the perovskite-type materials decreased the average oxygen concentration during the inert periods. In the inert periods following reduction in the presence of SO₂, all perovskite-type materials showed an increase in average oxygen concentration in the inert period with a rise in temperature.

However, for undoped and Mg-doped materials, the average oxygen concentrations were considerably lower than the inert periods following a reduction in the absence of SO₂. Thus, it can be inferred that SO₂ had degraded the oxygen uncoupling properties of the investigated materials. Materials doped with both Mg and Ti materials showed no substantial difference in the average oxygen concentration following reduction in the presence of SO₂.

3.2 Reactivity of the oxygen carriers

Figure 4 shows a typical gas concentration and temperature profile during the third reduction and following oxidation periods at 1000°C for the C43MMg oxygen carrier with 50% CH₄-balance N₂. Initially, the carrier was oxidized in 5% O₂, however, when it was shifted to the inert (N₂) period, the oxygen concentration decreased steadily in the same way as shown in Figure 4 for the oxygen uncoupling tests. Upon fuel addition, the CO₂ evolved as methane was converted, while the oxygen concentration decreased to zero. After the complete conversion of fuel in the early part of the reduction period, some CH₄ and CO could be detected. There was a slight increase in temperature during the reduction period and a greater increase in temperature during the oxidation period as a result of the overall exothermicity of the occurring reactions. As shown previously,²⁴ the reduction of similar perovskite-structured materials caused by methane has occurred by means of a combination of two reactions: (1) direct reaction of methane with the solid particles (via CLC), and (2) the reaction of methane with the gaseous oxygen released from the carrier (via CLOU).

A large number of chemical reactions could be written for the SO₂-CH₄-O₂ reaction system. Preliminary equilibrium calculations using HSC Chemistry[®] (ver. 5.11)⁵⁷ indicates that under the experimental conditions used in this investigation, i.e. the sub-stoichiometric combustion of CH₄ in the presence of SO₂, H₂S should be formed. Therefore several basic experiments were carried out to investigate the reactions that may possibly occur, the products of the SO₂-CH₄-O₂ reaction system, and to ensure that a mass balance for sulphur over the reactor system could be obtained. Initially, the absence of homogenous reactions in the system or any influence from the reactor system was confirmed by passing the 0.5% SO₂ and 50% CH₄-balance N₂ feeding gas mixture through a reactor without a bed of oxygen carrier particles at 950°C. Following this, a set of experiments with partial and complete combustion of methane in the presence of SO₂ at temperatures of 900 and 1000°C was performed using an empty reactor. In this set of experiments, oxygen was added to the feeding gas mixture in stoichiometric and sub-stoichiometric conditions to emulate oxygen release from the particles. The rationale for this experiment was to investigate whether reduced sulphur compounds such

as COS, H₂S or S could be formed by means of gas-phase reactions, which would need to be taken into account in the sulphur mass balance. Therefore, it would be possible to confirm whether the loss of sulphur in the effluent was due to the formation of reduced sulphur species or due to a reaction with the actual perovskite-structured material. No reduced sulphur species were found when running the experiment in an empty reactor since all SO₂ introduced to the reactor was detected by the analyser in the form of SO₂, meaning that a 100% mass balance for sulphur could be achieved.

It has also been reported that perovskite-type materials possess catalytic activity for the reduction of SO₂ to H₂S, COS and S in the presence of a reducing gas such as methane.^{58, 59} In order to examine whether reduced sulphur species may form in the presence of the investigated materials, several preliminary reactivity cycles were carried out. To do this, the gas following the first filter filled with Mg(ClO₄)₂ as the drying agent was led into another heated oven at 900°C where additional oxygen was provided to oxidize all the compounds to their fully oxidized state. This meant that the remaining unconverted CO and CH₄ as well as any reduced sulphur species that may have been produced as a result of the bed material's catalytic activity for the reduction of SO₂, would be oxidized to CO₂, H₂O and SO₂. An additional filter with Mg(ClO₄)₂ as the drying agent was also placed after this second oxidation step. By-pass mechanisms using two-way valves allowed bypassing the second oxidation step and therefore leading the effluent gas from the reactor directly to the analyser. Thus, a fuel cycle with 50% CH₄ and 0.5% SO₂-balance N₂ was performed using the C45M-1300 oxygen carrier at both 900 and 1000°C. The total SO₂ yield was measured in two different ways: (1) through the second heated oven, and (2) through bypassing the second oven and leading the off-gas directly to the analyser. The total SO₂ yield was determined by integrating the area under the SO₂ curve. The total SO₂ yield was the same in both cases and at both temperatures which indicated that reduced sulphur species were not created during the reduction phase, even in the presence of a perovskite-type oxygen carrier in the bed. Consequently, the second oxidation step was omitted in the remainder of the reactivity tests.

Figure 5 shows the concentration and temperature profiles for C43MMg during the fifth fuel cycle with 50% CH₄ and 0.5% SO₂-balance N₂ at 1000°C. By comparing Figure 5 with Figure 4, it can be seen that less methane had been converted, as shown by the lower CO₂ and higher CH₄ peaks when the oxygen carrier was exposed to SO₂ during the reduction phase. Only a small fraction of SO₂ had passed through the reactor during the reduction period, whereas in the subsequent inert and oxidation periods, more SO₂ was found in the off-gas. The oxidation

time until stable oxygen concentration (5%) was reached, was also shorter for the experiment in the presence of SO₂ than in the experiment with the absence of SO₂. This can be explained by the fact that more oxygen was consumed during the reduction of the material when SO₂ was absent than when the oxygen carrier was reduced in the presence of SO₂, likely due to deactivation of the oxygen carrier in the latter case. Possible mechanisms for the reaction of sulphur with the investigated perovskite-type oxygen carriers are discussed in Section 3.3.

Figure 6 shows the gas average gas yield, $\gamma_{CH_4,ave}$, and total SO₂ yield, η_{SO_2} , as a function of temperature during fuel cycles in the presence of SO₂ for C40MTMg at 900, 950 and 1000°C. It can be noted that there was a slight decrease in reactivity after every cycle. It was shown previously that a significant number of fuel cycles (~30) must be carried out in order to observe a significant decrease in reactivity caused by sulphur deactivation.⁵⁰ However, carrying out such a large number of cycles was outside the timeframe of this study because of the large number of investigated materials. It can also be observed that at 1000°C, approximately 80% of the introducing SO₂ passed through the reactor and was detected by the gas analyser. At 950°C this decreased to nearly 40% and at 900°C, only 10% of the introducing SO₂ reached the gas analyser. Consequently, it can be readily deduced that less SO₂ was adsorbed to and/or reacted with the oxygen carrier with an increase in temperature. This is in accordance with Figure 1, given the fact that the stable region of CaO increased with temperature, meaning that the driving force for CaSO₄ or CaS formation was weaker at high temperatures.

Figure 7 shows the total SO₂ yield, η_{SO_2} , as a function of temperature during fuel cycles with 50% CH₄ and 0.5% SO₂ for all investigated materials at 900, 950 and 1000°C. Similar to Figure 5, it can be inferred that the amount of SO₂ that passed through the reactor increased with an increase in temperature. Moreover, the total SO₂ yield, η_{SO_2} , increased with a decrease in the calcium content of the materials for both Mg- and Mg and Ti-doped materials. This could be expected since less calcium was available in the structure which could possibly result in the formation of CaSO₄ or CaS. It should be mentioned, however that this was not the case with undoped materials.

To facilitate the comparison between the reactivity of different oxygen carriers at different temperatures, the average gas yield, $\gamma_{CH_4,ave}$ is shown in Figure 8 for all of the investigated oxygen carriers in the presence and the absence of SO₂. Since $\gamma_{CH_4,ave}$ was stable during

reactivity testing in the absence of SO_2 , the $\gamma_{\text{CH}_4,ave}$ presented in Figure 8 is the average of gas conversion during three fuel cycles in the absence of SO_2 . However, as shown in Figure 6, $\gamma_{\text{CH}_4,ave}$ decreased slightly with cycling during reactivity experiments in the presence of SO_2 , likely as a result of sulphur deactivation. Therefore, the $\gamma_{\text{CH}_4,ave}$ presented in Figure 8 during reactivity testing in the presence of SO_2 is representative of the gas yield of the last cycle at each temperature, and not the average gas yield of all cycles at a given temperature. In Figure 8, three different effects can be discussed, i.e. the effect of calcium content, the effect of temperature and the effect of dopant, both during reduction in the presence and the absence of SO_2 . It can be seen that in the experiments in the absence of SO_2 , a lower calcium content in the materials generally resulted in less gas conversion. This would be expected since less $\text{CaMnO}_{3-\delta}$ is expected to be formed during synthesis in those materials. In the presence of SO_2 , the drop in gas conversion for oxygen carriers with lower calcium content was also less for the undoped and Mg-doped materials. This could be anticipated, too, due to less chance for CaSO_4 or CaS formation in samples with a lower calcium content. This can also be asserted by their higher total SO_2 yield, η_{SO_2} , as shown in Figure 7, compared to materials with higher calcium content. However, this was not the case for the doubly Mg and Ti-doped materials. Instead, for these materials it was possible to maintain a lower drop in reactivity for materials with higher calcium content, despite their lower total SO_2 yield, η_{SO_2} , as shown in Figure 7. It is unclear at this point, whether this could be attributed to the substitution of the B-site with Ti in these materials, consequently this requires additional study of the interaction of different perovskite-structured materials and sulphur species. The reactivity of most of the oxygen carriers increased with temperature both in the presence and the absence of SO_2 . However, it was also clear that reactivity decreased in the presence of SO_2 for all of the investigated oxygen carriers. The drop in reactivity increased at lower temperatures and could be as large as 50% at 900°C, whereas at 1000°C, the largest decrease in reactivity was about 20%. This again can be ascribed to the lower thermodynamic favourability of CaSO_4 or CaS formation at higher temperatures, as shown in Figure 1.

Since increasing the temperature had a more notable effect on the decrease in sulphur deactivation, additional experiments for the reactivity of three oxygen carriers were carried out at 1050°C, which are summarized in Figure 9. It is easily seen that at 1050°C, the decrease in reactivity following reduction in the presence of SO_2 became minimal at only 1%. Furthermore, the doubly Mg and Ti-doped material exhibited a lower decrease in reactivity in

the presence of SO₂ compared to undoped and singly Mg-doped materials. The total SO₂ yield, η_{SO_2} , at 1050°C could reach as high as 0.94. Experiments at even higher temperatures (e.g. 1100°C), could possibly result in a total SO₂ yield, η_{SO_2} , of 1, and consequently entirely avoid any sulphur deactivation. However, it should be mentioned that a slight deactivation in the reactivity of C50MMg in the absence of SO₂ has been reported already at 1050°C,³³ which could become more severe at 1100°C.

3.3 Mechanisms of sulphur reaction with the oxygen carriers

Possible mechanisms for the reaction of sulphur with the investigated perovskite-structured materials are discussed in the following. The first possible mechanism could be that CaS is formed during the reduction period via similar reactions to Eq. (10) and (11), given the highly reducing potential of CH₄, in accordance with Figure 1. However, in the inert period following reduction, SO₂ could be seen in the effluent, as shown in Figure 5, despite the absence of any oxygen which could possibly oxidize CaS to CaO and SO₂, via Eq. (2). This suggests that this mechanism cannot solely describe the formation of SO₂ in the inert period subsequent to reduction and instead CaSO₄ must be the source for the release of SO₂.

Another possible pathway could be that CaS reacts with CaSO₄ via Eq. (12) resulting in the formation of SO₂. This in particular could be valid in the later cycles after CaSO₄ had already formed in the material during earlier methane cycles in the presence of SO₂. However, this was not the case, since a similar concentration profile for SO₂ as shown in Figure 5, was also seen in the inert period of the first methane cycle in the presence of SO₂ at 1000°C, for which there was no CaSO₄ in the material from the beginning. Nevertheless, it may be possible that both CaS and CaSO₄ were formed during a reduction period. As shown in the early part of the reduction phase in Figure 5, some oxygen was present in the bed which could favour the formation of CaSO₄, while in the later part of the reduction, CaS formation was more favoured due to the absence of oxygen, see Figure 1.

It is worth noting that even 4 h inert (N₂) gas cycles for C45M did not show any SO₂ in the off-gas, which could indicate the spontaneous decomposition of CaSO₄ following several methane cycles in the presence of SO₂. This indicates that a sufficiently reducing environment is required to allow CaSO₄ to decompose. Thus, a third mechanism could be that the presence of a highly reduced bed material, e.g. CaMnO₂ or CaMnO_{2.5}, following the reduction period, increases the reducing potential in the reactor in the subsequent inert period, thus enforcing CaSO₄ to decompose. It is likely that the deactivation and subsequent partial regeneration of

the perovskite-type oxygen carriers occurred via either the second or the third mechanism or a combination of both. Both mechanisms can be seen as the decomposition of CaSO_4 , the reversed Eq. (4), made possible by the presence of compounds that can readily react with any surplus of oxygen, e.g. CaMnO_2 , $\text{CaMnO}_{2.5}$ or CaS . It can be speculated that such reactions may be facilitated by the high oxygen conductivity typical of perovskite materials.

3.4 Regeneration of the oxygen carriers following deactivation with SO_2

Figure 1 also implies that the perovskite-type oxygen carrier may be regenerable since CaSO_4 can decompose to CaO and SO_2 , where CaO can react again with Mn_3O_4 and reconstruct the $\text{CaMnO}_{3-\delta}$ phase. In this set of experiments, the C45M oxygen carrier which had already been subjected to 43 fuel cycles in the presence of SO_2 and as a result, the reactivity had decreased substantially compared to experiments in the absence of SO_2 , was used to investigate the potential for regeneration. Figure 10 shows the $\gamma_{\text{CH}_4,ave}$ as a function of cycle number at 1000°C in different conditions. The experiment consisted of seven fuel cycles with a considerably longer second inert period (~ 40 min) in the absence of SO_2 . The rationale for using a longer second inert period was to decompose as much CaSO_4 as possible. It can be observed that the $\gamma_{\text{CH}_4,ave}$ increased to approximately that of the experiment without the presence of SO_2 from the beginning, thus showing that the oxygen carrier could be regenerated. Similar observations have been reported for the partial regeneration of $\text{LaFe}_{0.8}\text{Cu}_{0.2}\text{O}_3$ catalysts in 5% H_2 in Ar.⁴² When SO_2 was again included in the reduction period, see cycles eight and nine, the reactivity decreased in a manner similar to that shown in Figure 8.

3.5 Attributes of the oxygen carriers before and after reactivity tests

Table 4 summarizes the physical and chemical characteristics of the investigated oxygen carrier particles before and after the reactivity testing. There was no significant change in the density and BET specific surface area of the particles and the observed minor changes can be considered as being within the margin of error for the methods used.

The oxygen capacity, R_o , for CLOU for most of the materials except those containing Mg and Ti were nearly constant at approximately 1%, irrespective of the calcium content. However, for the doubly Mg and Ti-doped oxygen carriers, the oxygen capacity for CLOU increased with the calcium content. This could indicate that the effect of Ti substitution in these materials is more pronounced in increasing the oxygen non-stoichiometry.

There was no change in the crystalline phase of any of the oxygen carriers after the reactivity test compared to their fresh counterparts, as determined with the XRD analysis. Figure 11 shows the XRD signatures of fresh and used samples as well as the signature after reactivity testing in the presence of SO₂ for C40MMg. In the case of used particles after reactivity testing in the presence of SO₂, no characteristic peaks could be attributed to CaSO₄ or CaS. This is not surprising given the low number of sulphur deactivation cycles, since it has been reported that a large number of cycles are needed in order to readily observe peaks associated with CaSO₄ during the deactivation of perovskite-structured materials with SO₂.³⁹ However, the intensity of the characteristic peaks for marokite (CaMn₂O₄) increased with a concomitant decrease in the intensity for peaks associated with the active perovskite, e.g. CaMnO_{3-δ}, in all samples following reactivity testing both in the presence and absence of SO₂. In all Mg-containing samples, MgO was also found as a separate phase, and was not incorporated into the perovskite structure, most likely due to a mismatch in the ionic radii of Mg and that of Mn,⁶⁰ which has also been reported elsewhere^{32, 33, 36} for CaMn_{0.9}Mg_{0.1}O_{3-δ} (C50MMg).

The ESEM images of fresh and used samples after reactivity testing in the presence and absence of SO₂ for the C43MTMg material are shown in Figure 12. The porosity and morphology of the particles did not seem to have been affected after the reactivity test. This was valid for all of the oxygen carriers investigated here.

Partial EDX analysis of the surface of the fresh and used samples after reactivity testing in the presence and absence of SO₂ is shown in Figure 13. Following the reactivity experiments in the presence of SO₂, a uniform distribution of the sulphur element could be found on the surface of the materials in addition to the inherent elements of the oxygen carrier, i.e. calcium, titanium, magnesium, manganese and oxygen. However, analysis of the bulk cross sections did not show the presence of the sulphur element, despite reports of the complete destruction of the perovskite bulk catalysts when deactivated with SO₂.⁴⁰⁻⁴² This could be again attributed to the low number of reactivity cycles in the presence of SO₂ in this study.

Only a few of the materials prepared in this study showed reasonable mechanical stability, as indicated by the crushing strength measured prior to the reactivity tests shown in Table 4. Figure 14 shows the rate of attrition of the used oxygen carriers in a jet-cup attrition rig for 1 h. In Table 5, the attrition index, A_i , defined as the slope of the attrition in the last 30 minutes of the test period, is shown for the oxygen carriers investigated. It can be seen that most of the investigated oxygen carriers have very similar attrition rates and are in an order similar to

$\text{CaMn}_{0.9}\text{Mg}_{0.1}\text{O}_{3-\delta}$ (C50MMg) which has shown excellent functionality in continuous operation in a 10 kW unit.³⁶ Consequently, equally good results could be expected for these materials. Nevertheless, experiments in continuous operation are required for confirmation.

4. Conclusion

Perovskite-structured oxygen carriers of the type $\text{Ca}_x\text{Mn}_{1-y}\text{M}_y\text{O}_{3-\delta}$ ($\text{M} = \text{Mg}, \text{Ti}$) were investigated for the CLOU process. The materials were prepared by spray drying, and the experiments were carried out in a batch fluidized-bed to evaluate the influence of calcium content, dopants (Mg and Ti) and operating temperature (900, 950, 1000 and 1050°C) on the oxygen uncoupling property and the reactivity of oxygen carriers with CH_4 in the presence and absence of SO_2 .

All of the oxygen carriers exhibited oxygen uncoupling behaviour. Their reactivity with methane was high and increased with temperature and calcium content, approaching complete gas yield at 1000°C. The reactivity decreased in the presence of SO_2 for all of the investigated oxygen carriers. Decreasing the calcium content in the materials generally resulted in less of decrease in reactivity in the presence of SO_2 , with the exception of materials doped with both Mg and Ti, where a higher resistance to sulphur deactivation could be maintained even at a higher calcium content. The drop in reactivity in the presence of SO_2 also decreased at higher temperatures and at 1050°C, the decrease in the reactivity of the Mg and Ti-doped material was minimal. Sulphur balance over the reactor system indicated that the fraction of the introduced SO_2 that passed through the reactor increased with temperature. It was shown that it is possible to regenerate the oxygen carriers during reduction in the absence of SO_2 . Most of the developed materials also showed relatively low attrition rates. Nevertheless, achieving higher sulphur tolerant perovskite-type oxygen carriers requires further study.

Acknowledgments

The research leading to these results has received funding from the European Research Council under the European Union's Seventh Framework Programme (FP7/2007-2013) / ERC grant agreement n° 291235. The authors also wish to acknowledge Chalmers University of Technology via the Energy Area of Advance for financial support for this research.

References

(1) Lewis, K. W.; Gilliland, E. R.; Sweeney, M. P. Gasification of Carbon Metal Oxides in a Fluidized Powder Bed. *Chem. Eng. Prog.* **1951**, 47 (5), 251-256.

- (2) Ishida, M.; Jin, H. A Novel Chemical-Looping Combustor without NO_x Formation. *Ind. Eng. Chem. Res.* **1996**, *35* (7), 2469-2472.
- (3) Ishida, M.; Jin, H. A new advanced power-generation system using chemical-looping combustion. *Energy* **1994**, *19* (4), 415-422.
- (4) Lyngfelt, A.; Leckner, B.; Mattisson, T. A fluidized-bed combustion process with inherent CO₂ separation; application of chemical-looping combustion. *Chem. Eng. Sci.* **2001**, *56* (10), 3101-3113.
- (5) Kronberger, B.; Johansson, E.; Löffler, G.; Mattisson, T.; Lyngfelt, A.; Hofbauer, H. A Two-Compartment Fluidized Bed Reactor for CO₂ Capture by Chemical-Looping Combustion. *Chem. Eng. Technol.* **2004**, *27* (12), 1318-1326.
- (6) Lyngfelt, A. Oxygen Carriers for Chemical Looping Combustion – 4000 h of Operational Experience. *Oil Gas Sci. Technol.* **2011**, *66* (2), 161-172
- (7) Lyngfelt, A. *Chemical looping combustion*; Chapter 20 in Fluidized-bed technologies for near-zero emission combustion and gasification; Scala, F. (Ed.), Woodhead Publishing Limited: Cambridge, 2013, 895-930
- (8) Lyngfelt, A. Chemical-looping combustion of solid fuels – Status of development. *Appl. Energy* **2014**, *113*, 1869-1873.
- (9) Hossain, M. M.; de Lasa, H. I. Chemical-looping combustion (CLC) for inherent CO₂ separations-a review. *Chem. Eng. Sci.* **2008**, *63* (18), 4433-4451.
- (10) Adanez, J.; Abad, A.; Garcia-Labiano, F.; Gayan, P.; de Diego, L. F. Progress in Chemical-Looping Combustion and Reforming technologies. *Progr. Energy Combust. Sci.* **2012**, *38* (2), 215-282.
- (11) Fan, L.-S.; Zeng, L.; Wang, W.; Luo, S. Chemical looping processes for CO₂ capture and carbonaceous fuel conversion – prospect and opportunity. *Energy & Environmental Science* **2012**, *5* (6), 7254-7280.
- (12) Brown, T. A.; Dennis, J. S.; Scott, S. A.; Davidson, J. F.; Hayhurst, A. N. Gasification and Chemical-Looping Combustion of a Lignite Char in a Fluidized Bed of Iron Oxide. *Energy Fuels* **2010**, *24* (5), 3034-3048.
- (13) Dennis, J. S.; Müller, C. R.; Scott, S. A. In situ gasification and CO₂ separation using chemical looping with a Cu-based oxygen carrier: Performance with bituminous coals. *Fuel* **2010**, *89* (9), 2353-2364.
- (14) Scott, S. A.; Dennis, J. S.; Hayhurst, A. N.; Brown, T. In situ gasification of a solid fuel and CO₂ separation using chemical looping. *AIChE J.* **2006**, *52* (9), 3325-3328.
- (15) Leion, H.; Mattisson, T.; Lyngfelt, A. Solid fuels in chemical-looping combustion. *Int. J. Greenhouse Gas Control* **2008**, *2* (2), 180-193.
- (16) Leion, H.; Mattisson, T.; Lyngfelt, A. The use of petroleum coke as fuel in chemical-looping combustion. *Fuel* **2007**, *86* (12-13), 1947-1958.
- (17) Mattisson, T.; Lyngfelt, A.; Leion, H. Chemical-looping with oxygen uncoupling for combustion of solid fuels. *Int. J. Greenhouse Gas Control* **2009**, *3* (1), 11-19.
- (18) Abad, A.; Adánez-Rubio, I.; Gayán, P.; García-Labiano, F.; de Diego, L. F.; Adánez, J. Demonstration of chemical-looping with oxygen uncoupling (CLOU) process in a 1.5 kW_{th} continuously operating unit using a Cu-based oxygen-carrier. *Int. J. Greenhouse Gas Control* **2012**, *6*, 189-200.
- (19) Gayán, P.; Adánez-Rubio, I.; Cuadrat, A.; Mendiara, T.; Abad, A.; García-Labiano, F.; De Diego, L.; Adánez, J. Use of Chemical-Looping processes for coal combustion with CO₂ capture. *Energy Procedia* **2013**.
- (20) Arjmand, M.; Keller, M.; Leion, H.; Mattisson, T.; Lyngfelt, A. Oxygen Release and Oxidation Rates of MgAl₂O₄-Supported CuO Oxygen Carrier for Chemical-Looping Combustion with Oxygen Uncoupling (CLOU). *Energy Fuels* **2012**, *26* (11), 6528-6539.

- (21) Mattisson, T. Materials for Chemical-Looping with Oxygen Uncoupling. *ISRN Chemical Engineering* **2013**, 1-19.
- (22) Rydén, M.; Leion, H.; Mattisson, T.; Lyngfelt, A. Combined oxides as oxygen-carrier material for chemical-looping with oxygen uncoupling. *Appl. Energy* **2013**, *113*, 1924-1932.
- (23) Imtiaz, Q.; Hosseini, D.; Müller, C. R. Review of Oxygen Carriers for Chemical Looping with Oxygen Uncoupling (CLOU): Thermodynamics, Material Development, and Synthesis. *Energy Technology* **2013**, *1* (11), 633-647.
- (24) Arjmand, M.; Hedayati, A.; Azad, A.-M.; Leion, H.; Rydén, M.; Mattisson, T. $\text{Ca}_x\text{La}_{1-x}\text{Mn}_{1-y}\text{M}_y\text{O}_{3-\delta}$ (M = Mg, Ti, Fe, or Cu) as Oxygen Carriers for Chemical-Looping with Oxygen Uncoupling (CLOU). *Energy Fuels* **2013**, *27* (8), 4097-4107.
- (25) Fossdal, A.; Bakken, E.; Øye, B. A.; Schøning, C.; Kaus, I.; Mokkelbost, T.; Larring, Y. Study of inexpensive oxygen carriers for chemical looping combustion. *Int. J. Greenhouse Gas Control* **2011**, *5* (3), 483-488.
- (26) Sarshar, Z.; Kleitz, F.; Kaliaguine, S. Novel oxygen carriers for chemical looping combustion: $\text{La}_{1-x}\text{Ce}_x\text{BO}_3$ (B = Co, Mn) perovskites synthesized by reactive grinding and nanocasting. *Energy & Environmental Science* **2011**, *4* (10), 4258-4269.
- (27) Sarshar, Z.; Sun, Z.; Zhao, D.; Kaliaguine, S. Development of Sinter-Resistant Core-Shell $\text{LaMn}_x\text{Fe}_{1-x}\text{O}_3@m\text{SiO}_2$ Oxygen Carriers for Chemical Looping Combustion. *Energy Fuels* **2012**, *26* (5), 3091-3102.
- (28) Readman, J. E.; Olafsen, A.; Larring, Y.; Blom, R. $\text{La}_{0.8}\text{Sr}_{0.2}\text{Co}_{0.2}\text{Fe}_{0.8}\text{O}_{3-\delta}$ as a potential oxygen carrier in a chemical looping type reactor, an in-situ powder X-ray diffraction study. *J. Mater. Chem.* **2005**, *15* (19), 1931-1937.
- (29) Leion, H.; Larring, Y.; Bakken, E.; Bredesen, R.; Mattisson, T.; Lyngfelt, A. Use of $\text{CaMn}_{0.875}\text{Ti}_{0.125}\text{O}_3$ as Oxygen Carrier in Chemical-Looping with Oxygen Uncoupling. *Energy Fuels* **2009**, *23* (10), 5276-5283.
- (30) Rydén, M.; Lyngfelt, A.; Mattisson, T.; Chen, D.; Holmen, A.; Bjørgum, E. Novel oxygen-carrier materials for chemical-looping combustion and chemical-looping reforming; $\text{La}_x\text{Sr}_{1-x}\text{Fe}_y\text{Co}_{1-y}\text{O}_{3-\delta}$ perovskites and mixed-metal oxides of NiO, Fe_2O_3 and Mn_3O_4 . *Int. J. Greenhouse Gas Control* **2008**, *2* (1), 21-36.
- (31) Noorman, S.; Gallucci, F.; van Sint Annaland, M.; Kuipers, J. A. M. Experimental Investigation of Chemical-Looping Combustion in Packed Beds: A Parametric Study. *Ind. Eng. Chem. Res.* **2011**, *50* (4), 1968-1980.
- (32) Hallberg, P.; Jing, D.; Rydén, M.; Mattisson, T.; Lyngfelt, A. Chemical Looping Combustion and Chemical Looping with Oxygen Uncoupling Experiments in a Batch Reactor Using Spray-Dried $\text{CaMn}_{1-x}\text{MxO}_{3-\delta}$ (M = Ti, Fe, Mg) Particles as Oxygen Carriers. *Energy Fuels* **2013**, *27* (3), 1473-1481.
- (33) Jing, D.; Mattisson, T.; Leion, H.; Rydén, M.; Lyngfelt, A. Examination of Perovskite Structure $\text{CaMnO}_{3-\delta}$ with MgO Addition as Oxygen Carrier for Chemical Looping with Oxygen Uncoupling Using Methane and Syngas. *International Journal of Chemical Engineering* **2013**, *2013*, 1-16.
- (34) de Diego, L. F.; Abad, A.; Cabello, A.; Gayan, P.; Garcia-Labiano, F.; Adanez, J. Reduction and Oxidation Kinetics of a $\text{CaMn}_{0.9}\text{Mg}_{0.1}\text{O}_{3-\delta}$ Oxygen Carrier for Chemical Looping Combustion. *Ind. Eng. Chem. Res.* **2014**, *53* (1), 87-103.
- (35) Rydén, M.; Lyngfelt, A.; Mattisson, T. $\text{CaMn}_{0.875}\text{Ti}_{0.125}\text{O}_3$ as oxygen carrier for chemical-looping combustion with oxygen uncoupling (CLOU) – Experiments in a continuously operating fluidized-bed reactor system. *Int. J. Greenhouse Gas Control* **2011**, *5* (2), 356-366.
- (36) Källén, M.; Rydén, M.; Dueso, C.; Mattisson, T.; Lyngfelt, A. $\text{CaMn}_{0.9}\text{Mg}_{0.1}\text{O}_{3-\delta}$ as Oxygen Carrier in a Gas-Fired 10 kW_{th} Chemical-Looping Combustion Unit. *Ind. Eng. Chem. Res.* **2013**, *52* (21), 6923-6932.

- (37) Koponen, M. J.; Venäläinen, T.; Suvanto, M.; Kallinen, K.; Kinnunen, T.-J. J.; Härkönen, M.; Pakkanen, T. A. Methane conversion and SO₂ resistance of LaMn_{1-x}Fe_xO₃ (x = 0.4, 0.5, 0.6, 1) perovskite catalysts promoted with palladium. *J. Mol. Catal. A: Chem.* **2006**, *258* (1–2), 246-250.
- (38) Rosso, I.; Saracco, G.; Specchia, V.; Garrone, E. Sulphur poisoning of LaCr_{0.5-x}Mn_xMg_{0.5}O₃·yMgO catalysts for methane combustion. *Applied Catalysis B: Environmental* **2003**, *40* (3), 195-205.
- (39) Alifanti, M.; Auer, R.; Kirchnerova, J.; Thyron, F.; Grange, P.; Delmon, B. Activity in methane combustion and sensitivity to sulfur poisoning of La_{1-x}Ce_xMn_{1-y}Co_yO₃ perovskite oxides. *Applied Catalysis B: Environmental* **2003**, *41* (1–2), 71-81.
- (40) Zhu, Y.; Tan, R.; Feng, J.; Ji, S.; Cao, L. The reaction and poisoning mechanism of SO₂ and perovskite LaCoO₃ film model catalysts. *Applied Catalysis A: General* **2001**, *209* (1–2), 71-77.
- (41) Wang, H.; Zhu, Y.; Tan, R.; Yao, W. Study on the Poisoning Mechanism of Sulfur Dioxide for Perovskite La_{0.9}Sr_{0.1}CoO₃ Model Catalysts. *Catal. Lett.* **2002**, *82* (3–4), 199-204.
- (42) Zhang, R.; Alamdari, H.; Kaliaguine, S. SO₂ poisoning of LaFe_{0.8}Cu_{0.2}O₃ perovskite prepared by reactive grinding during NO reduction by C₃H₆. *Applied Catalysis A: General* **2008**, *340* (1), 140-151.
- (43) Tejuca, L. G.; Fierro, J. L. G. *Properties and Applications of Perovskite-Type Oxides*; (Ed.), Marcel Dekker: New York, 1993.
- (44) Li, W.; Dai, H.; Lieu, Y., Improving SO₂ Resistance of Base Metal Perovskite Type Oxidation Catalyst. In *Stud. Surf. Sci. Catal.*, Guzzi, L.; Solymosi, f.; Tétéyi, P., Eds. Elsevier: Budapest, 1993; Vol. 75, pp 1793-1796.
- (45) Rosso, I.; Saracco, G.; Specchia, V. Tackling the problem of sulfur poisoning of perovskite catalysts for natural gas combustion. *Korean J. Chem. Eng.* **2003**, *20* (2), 222-229.
- (46) Hansen, P. F. B.; Dam-Johansen, K.; Østergaard, K. High-temperature reaction between sulphur dioxide and limestone-V. The effect of periodically changing oxidizing and reducing conditions. *Chem. Eng. Sci.* **1993**, *48* (7), 1325-1341.
- (47) Fernández, M. J.; Lyngfelt, A.; Steenari, B. M. Reaction between limestone and SO₂ under conditions alternating between oxidizing and reducing. The effect of the SO₂ concentration. *J. Inst. Energy* **2000**, *73* (495), 119-125.
- (48) Mattisson, T.; Lyngfelt, A. The reaction between sulphur dioxide and limestone under periodically changing oxidising and reducing conditions – The effect of reducing gases. *J. Inst. Energy* **1998**, *71* (489), 190-196.
- (49) Bale, C. W.; Bélisle, E.; Chartrand, P.; Decterov, S. A.; Eriksson, G.; Hack, K.; Jung, I. H.; Kang, Y. B.; Melançon, J.; Pelton, A. D.; Robelin, C.; Petersen, S. FactSage thermochemical software and databases – recent developments. *Calphad* **2009**, *33* (2), 295-311.
- (50) Sundqvist, S.; Leion, H.; Rydén, M.; Lyngfelt, A.; Mattisson, T. CaMn_{0.875}Ti_{0.125}O_{3-δ} as an Oxygen Carrier for Chemical-Looping with Oxygen Uncoupling (CLOU) – Solid-Fuel Testing and Sulfur Interaction. *Energy Technology* **2013**, *1* (5–6), 338-344.
- (51) Adánez-Rubio, I.; Arjmand, M.; Leion, H.; Gayán, P.; Abad, A.; Mattisson, T.; Lyngfelt, A. Investigation of Combined Supports for Cu-Based Oxygen Carriers for Chemical-Looping with Oxygen Uncoupling (CLOU). *Energy Fuels* **2013**, *27* (7), 3918-3927.
- (52) Rydén, M.; Moldenhauer, P.; Lindqvist, S.; Mattisson, M.; Lyngfelt, A. Measuring attrition resistance of oxygen carrier particles for chemical-looping combustion with the jet cup method. *Submitted for publication* **2014**.
- (53) Arjmand, M.; Azad, A.-M.; Leion, H.; Lyngfelt, A.; Mattisson, T. Prospects of Al₂O₃ and MgAl₂O₄-Supported CuO Oxygen Carriers in Chemical-Looping Combustion (CLC) and

- Chemical-Looping with Oxygen Uncoupling (CLOU). *Energy Fuels* **2011**, 25 (11), 5493-5502.
- (54) Arjmand, M.; Azad, A.-M.; Leion, H.; Mattisson, T.; Lyngfelt, A. Evaluation of CuAl_2O_4 as an Oxygen Carrier in Chemical-Looping Combustion. *Ind. Eng. Chem. Res.* **2012**, 51 (43), 13924-13934.
- (55) Perry, R. H.; Green, D. W. *Perry's Chemical Engineering Handbook*; (Ed.), 7th ed.; McGraw-Hill 1997,
- (56) Kunii, D.; Levenspiel, O. *Fluidization Engineering*; 2nd (Ed.), Butterworth-Heinemann: Boston, 1991,
- (57) HSC Chemistry 5.0, Chemical Reaction and Equilibrium Software with Extensive Thermochemical Database. In Outokumpu Research Oy: Pori, Finland, 2002.
- (58) Hibbert, D. B.; Tseung, A. C. C. The reduction of sulphur dioxide by carbon monoxide on a $\text{La}_{0.5}\text{Sr}_{0.5}\text{CoO}_3$ catalyst. *J. Chem. Technol. Biotechnol.* **1979**, 29 (12), 713-722.
- (59) Hibbert, D. B. Reduction of Sulfur Dioxide on Perovskite Oxides. *Catalysis Reviews* **1992**, 34 (4), 391-408.
- (60) Shannon, R. D. Revised effective ionic radii and systematic studies of interatomic distances in halides and chalcogenides. *Acta Crystallographica Section A* **1976**, 32 (5), 751-767.

Tables

Table 1 Possible reaction pathways in the Ca–S–O system in oxidizing and reducing (CO and H₂) environments.

Oxidizing conditions	
(2)	$\text{CaS} + 3/2 \text{O}_2 \rightarrow \text{CaO} + \text{SO}_2$
(3)	$\text{CaS} + 2 \text{O}_2 \rightarrow \text{CaSO}_4$
(4)	$\text{CaO} + 1/2 \text{O}_2 + \text{SO}_2 \rightarrow \text{CaSO}_4$
Reducing conditions*	
(5)	$\text{CaSO}_4 + \text{CO} \rightarrow \text{CaO} + \text{SO}_2 + \text{CO}_2$
(6)	$\text{CaSO}_4 + \text{H}_2 \rightarrow \text{CaO} + \text{SO}_2 + \text{H}_2\text{O}$
(7)	$\text{CaSO}_4 + 4 \text{H}_2 \rightarrow \text{CaO} + 4 \text{H}_2\text{S} + 3\text{H}_2\text{O}$
(8)	$\text{CaSO}_4 + 4 \text{CO} \rightarrow \text{CaS} + 4 \text{CO}_2$
(9)	$\text{CaSO}_4 + 4 \text{H}_2 \rightarrow \text{CaS} + 4 \text{H}_2\text{O}$
(10)	$\text{CaO} + \text{SO}_2 + 3 \text{CO} \rightarrow \text{CaS} + 3 \text{CO}_2$
(11)	$\text{CaO} + \text{SO}_2 + 3 \text{H}_2 \rightarrow \text{CaS} + 3 \text{H}_2\text{O}$
(12)	$\text{CaS} + 3\text{CaSO}_4 \rightarrow 4\text{CaO} + 4\text{SO}_2$

* Hydrocarbons such as CH₄ could replace CO or H₂ as a reducing agent in reactions (5)–(11).

Table 2 Oxygen carriers prepared in this study.

Oxygen carrier*	Nominal molar composition†	Synthesis composition [wt.%]
C49M	$\text{CaMnO}_{3-\delta}$	50.7% Mn ₃ O ₄ , 49.3% Ca(OH) ₂
C45M	$\text{Ca}_{0.83}\text{MnO}_{3-\delta}$	55.3% Mn ₃ O ₄ , 44.7% Ca(OH) ₂
C50MMg	$\text{CaMn}_{0.90}\text{Mg}_{0.10}\text{O}_{3-\delta}$	46.8% Mn ₃ O ₄ , 50.5% Ca(OH) ₂ , 2.7% MgO
C46MMg	$\text{Ca}_{0.85}\text{Mn}_{0.90}\text{Mg}_{0.10}\text{O}_{3-\delta}$	50.6% Mn ₃ O ₄ , 46.4% Ca(OH) ₂ , 3.0% MgO
C43MMg	$\text{Ca}_{0.75}\text{Mn}_{0.90}\text{Mg}_{0.10}\text{O}_{3-\delta}$	53.5% Mn ₃ O ₄ , 43.3% Ca(OH) ₂ , 3.1% MgO
C40MMg	$\text{Ca}_{0.65}\text{Mn}_{0.90}\text{Mg}_{0.10}\text{O}_{3-\delta}$	56.8% Mn ₃ O ₄ , 39.9% Ca(OH) ₂ , 3.3% MgO
C50MTMg	$\text{CaMn}_{0.775}\text{Mg}_{0.10}\text{Ti}_{0.125}\text{O}_{3-\delta}$	40.1% Mn ₃ O ₄ , 50.4% Ca(OH) ₂ , 2.7% MgO, 6.8% TiO ₂
C46MTMg	$\text{Ca}_{0.85}\text{Mn}_{0.775}\text{Mg}_{0.10}\text{Ti}_{0.125}\text{O}_{3-\delta}$	43.4% Mn ₃ O ₄ , 46.3% Ca(OH) ₂ , 3.0% MgO, 7.3% TiO ₂
C43MTMg	$\text{Ca}_{0.75}\text{Mn}_{0.775}\text{Mg}_{0.10}\text{Ti}_{0.125}\text{O}_{3-\delta}$	45.9% Mn ₃ O ₄ , 43.2% Ca(OH) ₂ , 3.1% MgO, 7.8% TiO ₂
C40MTMg	$\text{Ca}_{0.65}\text{Mn}_{0.775}\text{Mg}_{0.10}\text{Ti}_{0.125}\text{O}_{3-\delta}$	48.7% Mn ₃ O ₄ , 39.7% Ca(OH) ₂ , 3.3% MgO, 8.2% TiO ₂

* Example of nomenclature for the oxygen carriers: C46MTMg, C46: ~46 wt.% Ca(OH)₂; M: Mn₃O₄; T: TiO₂; Mg: MgO.

† The nominal molar composition is an empirical composition of the samples assuming formation of perovskite-structured materials.

Table 3 Experimental scheme used for evaluating the reactivity and oxygen release ability of the investigated materials in the presence and absence of SO₂.

No. of cycles	Inert/reducing gas	Time during inert period for CLOU [s]	Time during inert purge [s]	Time during reduction period [s]	Temperature [°C]
3	50% CH ₄ – balance N ₂	–	60	20	900
3	N ₂	360	–	–	900
3	50% CH ₄ – balance N ₂	–	60	20	950
3	N ₂	360	–	–	950
3	50% CH ₄ – balance N ₂	–	60	20	1000
3	N ₂	360	–	–	1000
5	50% CH ₄ – 0.5% SO ₂ – balance N ₂	–	60	20	1000
3	N ₂	360	–	–	1000
5	50% CH ₄ – 0.5% SO ₂ – balance N ₂	–	60	20	950
3	N ₂	360	–	–	950
5	50% CH ₄ – 0.5% SO ₂ – balance N ₂	–	60	20	900
3	N ₂	360	–	–	900

Table 4 Physical and chemical characteristics of the investigated oxygen carriers as prepared and following reactivity testing in the absence of SO₂.

Oxygen carrier	Bulk density [g/cm ³]*		BET specific surface area [m ² /g]*		Oxygen capacity for CLOU at 1000°C, R _o [%]	Crystalline phases detected by XRD
	Fresh	Used	Fresh	Used		
C49M	1.4	1.6	0.28	0.25	1.04	CaMnO _{2.98} , CaMn ₂ O ₄
C45M	1.3	1.3	0.27	0.42	1.05	CaMnO _{2.80} , CaMn ₂ O ₄
C50MMg	1.5	1.5	0.37	0.39	0.94	CaMnO _{2.80} , CaMn ₂ O ₄ , MgO
C46MMg	1.4	1.4	0.25	0.02	1.00	CaMnO _{2.97} , CaMn ₂ O ₄ , MgO
C43MMg	1.1	1.3	0.4	0.22	0.99	CaMnO _{2.98} , CaMn ₂ O ₄ , MgO
C40MMg	0.9	1.0	0.47	0.57	0.98	CaMnO _{2.98} , CaMn ₂ O ₄ , MgO
C50MTMg	1.6	1.5	0.33	0.29	1.58	CaMn _{0.7} Ti _{0.3} O _{2.94} , MgO
C46MTMg	1.4	1.4	0.29	0.05	1.50	CaMn _{0.7} Ti _{0.3} O _{2.94} , CaMn ₂ O ₄ , MgO
C43MTMg	1.3	1.4	0.29	0.27	1.01	CaMn _{0.7} Ti _{0.3} O _{2.94} , CaMn ₂ O ₄ , MgO
C40MTMg	1.2	1.3	0.27	0.31	0.86	CaMn _{0.7} Ti _{0.3} O _{2.94} , CaMn ₂ O ₄ , MgO

Table 5 Attrition rates of the investigated oxygen carriers after reactivity testing and their corresponding crushing strength (CS) in the fresh state.

Oxygen carrier	Attrition rate, A_i [wt.%/h]	Crushing strength (CS) [N]
C49M	3.6	0.47
C45M	10.8	0.42
C50MMg	8.4	1.4
C46MMg	4.8	0.30
C43MMg	7.8	0.50
C40MMg	3.6	0.23
C50MTMg	8.2	1.4
C46MTMg	3.6	1.01
C43MTMg	7.8	1.37
C40MTMg	6.6	0.73

Figures

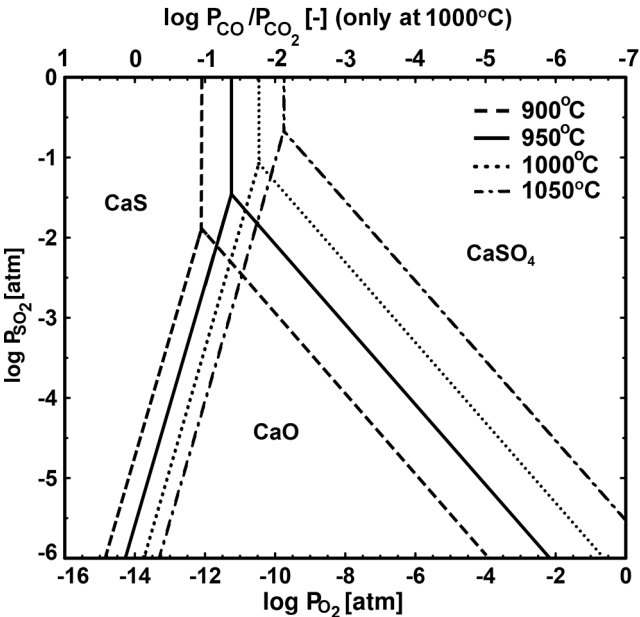


Figure 1 Predominance diagram for the system Ca–S–O showing the stability regions of CaS, CaSO₄ and CaO between 900 and 1050°C. The CO/CO₂ ratio corresponding to the log P_{O₂} at 1000°C is also shown in the diagram.

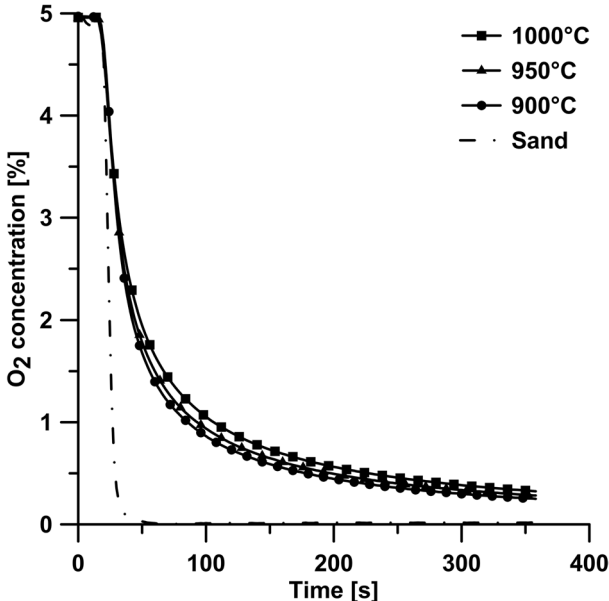


Figure 2 Oxygen profiles for inert cycle at 900, 950 and 1000°C using C46MTMg as bed material.

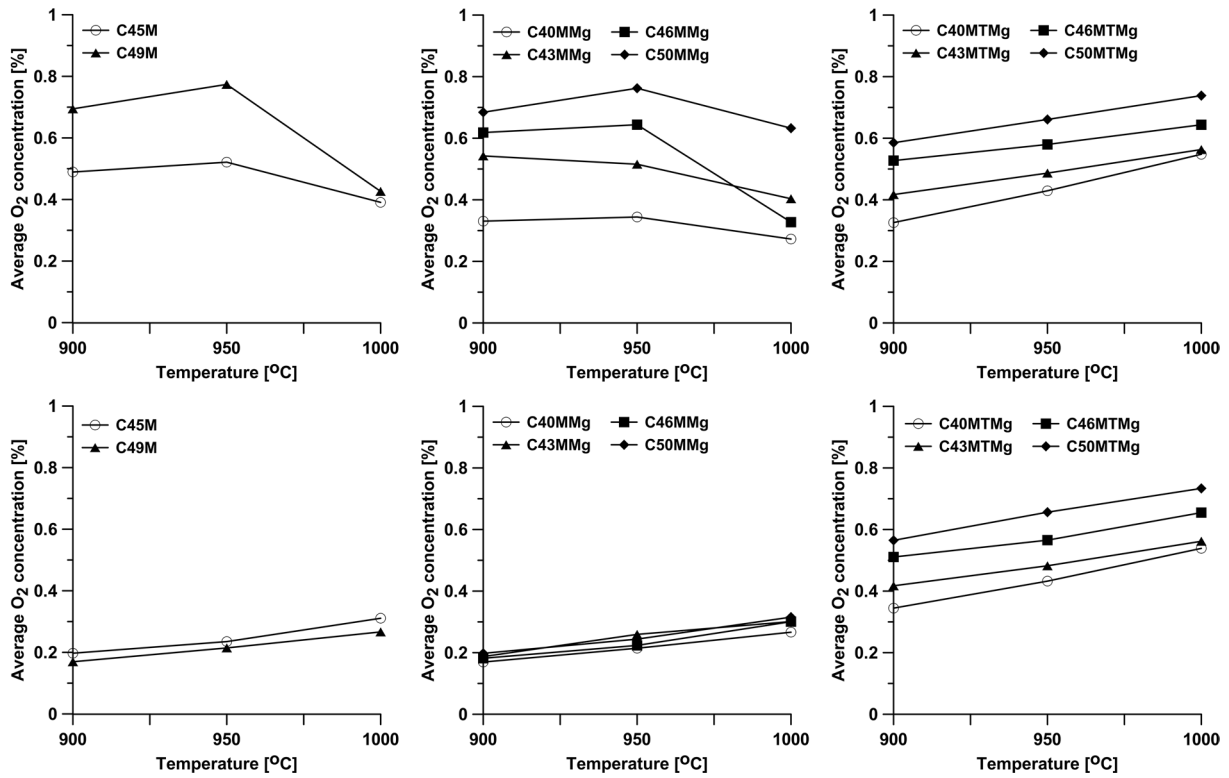


Figure 3 Average oxygen concentration as function of temperature during inert cycles for all investigated oxygen carriers following fuel cycles with (upper row) 50% CH₄-rest N₂ and (bottom row) 50% CH₄ and 0.5% SO₂-rest N₂ at 900, 950 and 1000°C.

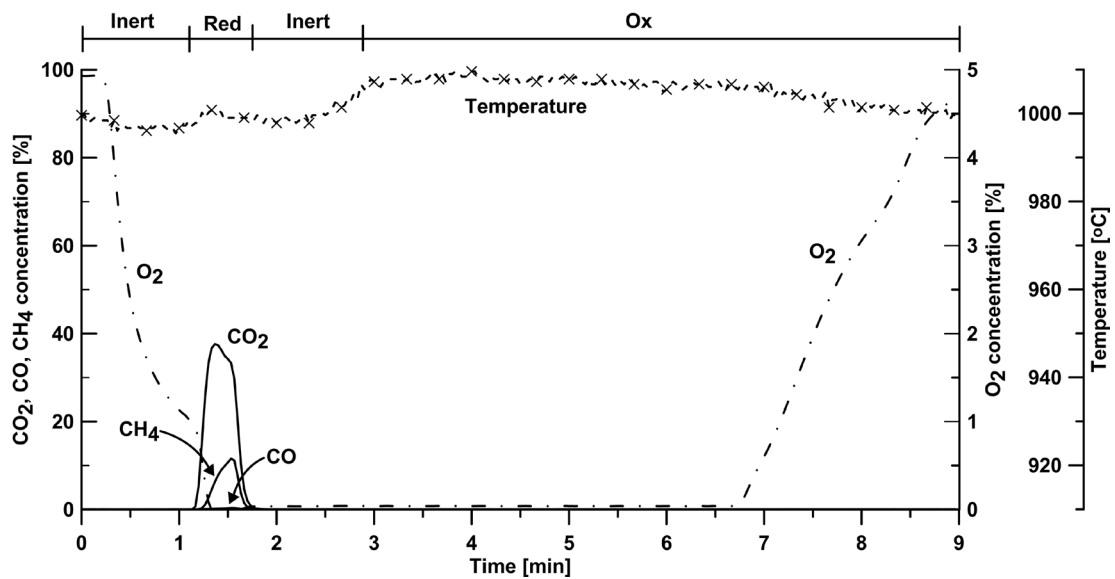


Figure 4 Gas concentration and temperature profile for C43MMg particle during third fuel cycle with 50% CH₄ (balance N₂) for 20 s at 1000°C.

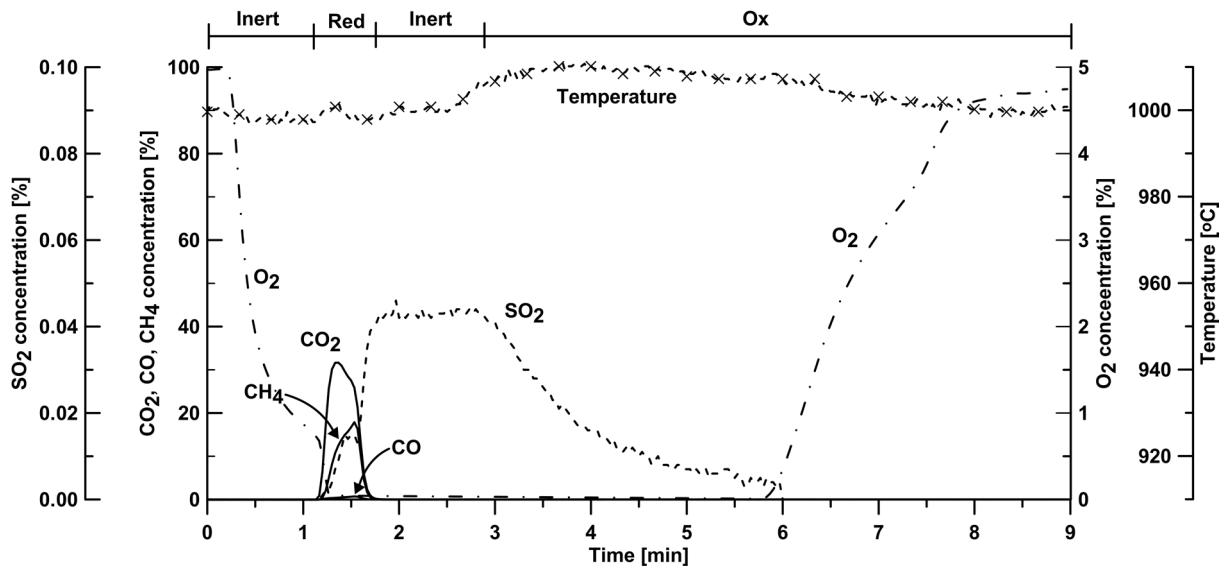


Figure 5 Gas concentration and temperature profile for C43MMg particle during fifth fuel cycle with 50% CH₄ and 0.5% SO₂-rest N₂ for 20 s at 1000°C.

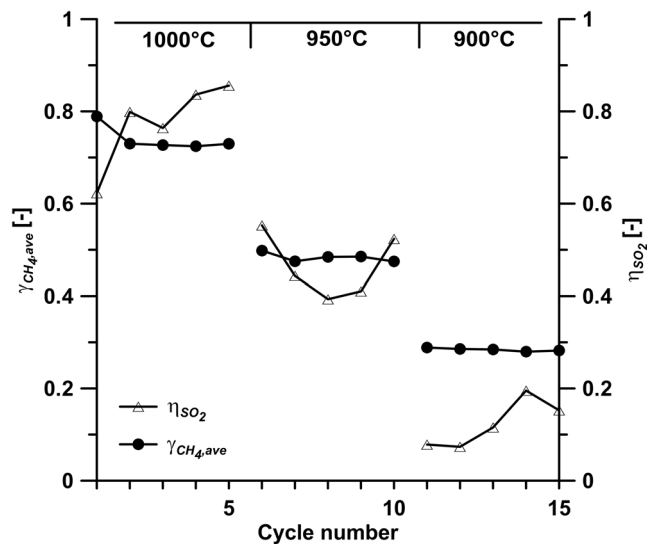


Figure 6 Average gas yield, $\gamma_{CH_4,ave}$, and total SO₂ yield, η_{SO_2} , as function of temperature during fuel cycles with 50% CH₄ and 0.5% SO₂-rest N₂ for C40MTMg as bed material at 900, 950 and 1000°C.

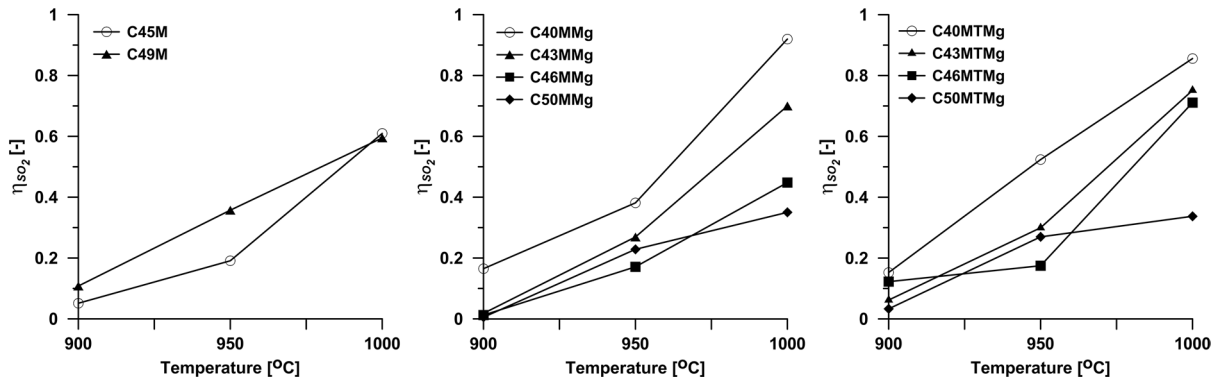


Figure 7 Total SO_2 yield, η_{SO_2} , as function of temperature during fuel cycles for all investigated oxygen carriers using 50% CH_4 and 0.5% SO_2 -rest N_2 at 900, 950 and 1000°C.

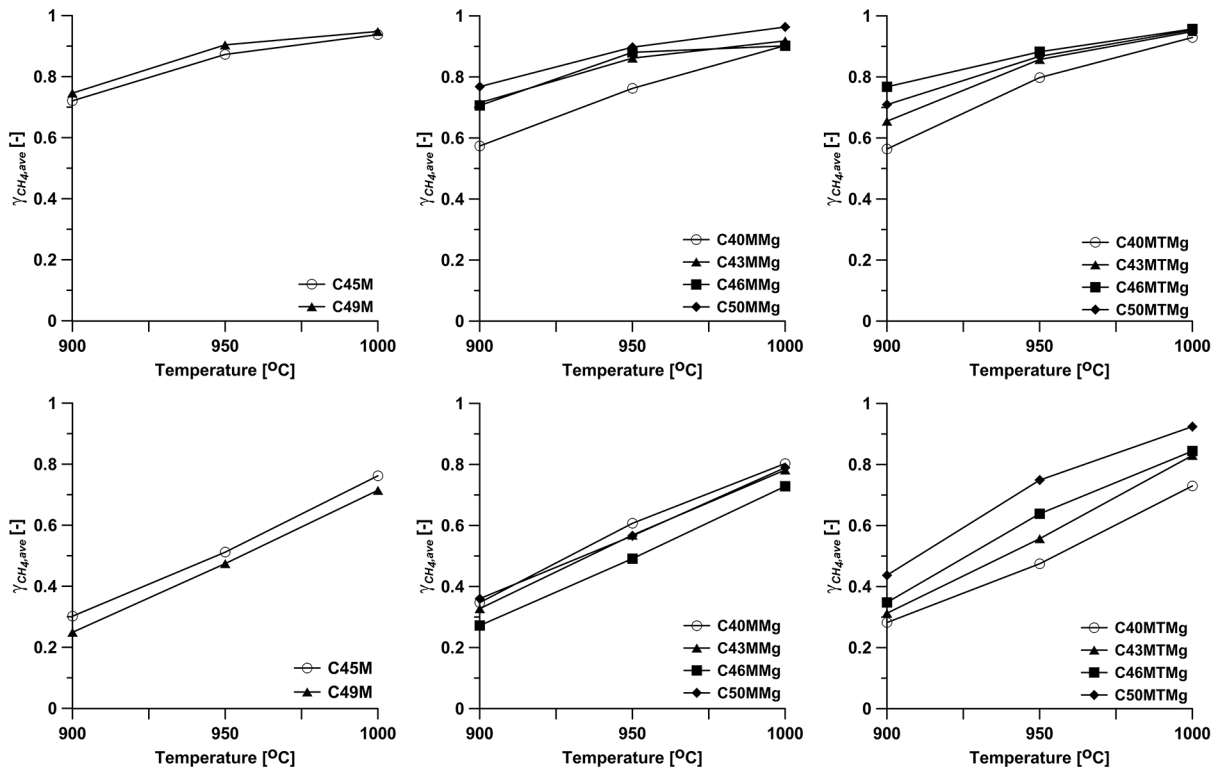


Figure 8 Average gas yield for CH_4 , $\gamma_{\text{CH}_4,ave}$, as function of temperature during fuel cycles for all investigated oxygen carriers using (upper row) 50% CH_4 -rest N_2 and (bottom row) 50% CH_4 and 0.5% SO_2 -rest N_2 at 900, 950 and 1000°C.

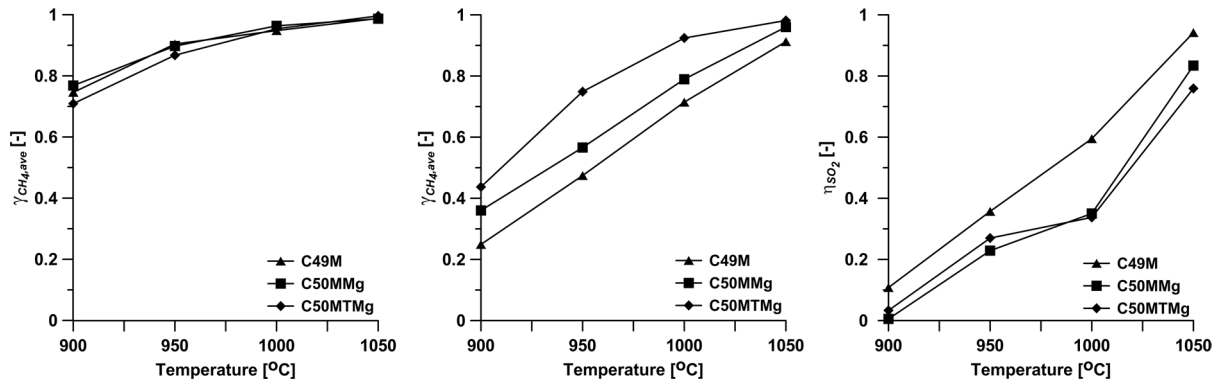


Figure 9 Average gas yield for CH₄, $\gamma_{CH_4,ave}$, during fuel cycles for C49M, C50MMg and C50MTMg oxygen carriers using (left) 50% CH₄-rest N₂ and (middle) 50% CH₄ and 0.5% SO₂-rest N₂ and (right) their respective total SO₂ yield, η_{SO_2} , at 900, 950, 1000 and 1050°C.

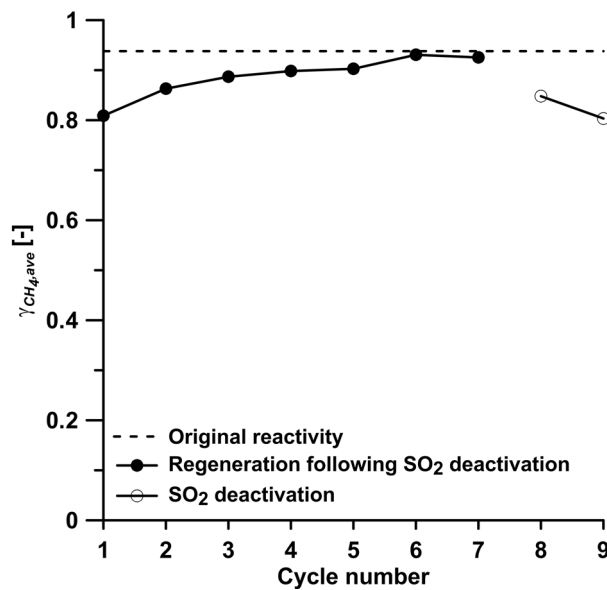


Figure 10 Average gas yield for CH₄, $\gamma_{CH_4,ave}$, as function of cycle number for C45M at 1000°C during regeneration and following sulphur deactivation of oxygen carrier.

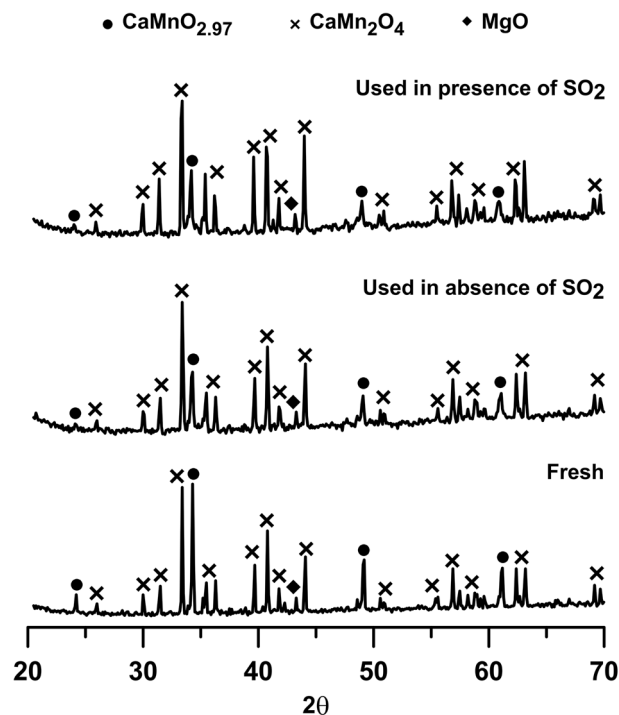


Figure 11 Comparative XRD signatures of (bottom) fresh and used in (middle) absence and (top) presence of SO_2 for C40MMg following oxidation in 5% O_2 stream.

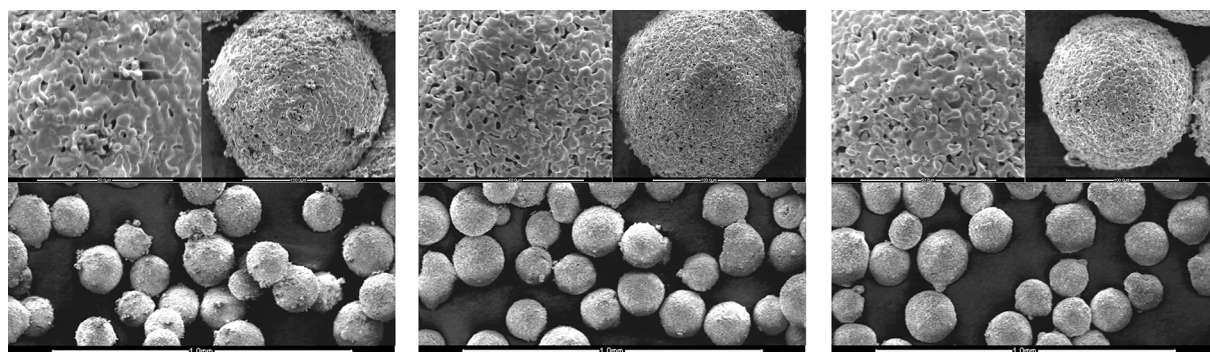


Figure 12 ESEM images of (left) fresh C43MTMg and particles subject to reactivity in the (middle) absence of SO_2 and (right) presence of SO_2 for particles. The size bars for the images with higher magnification are 50 and 100 μm , while those of the images with lower magnification are 1 mm.

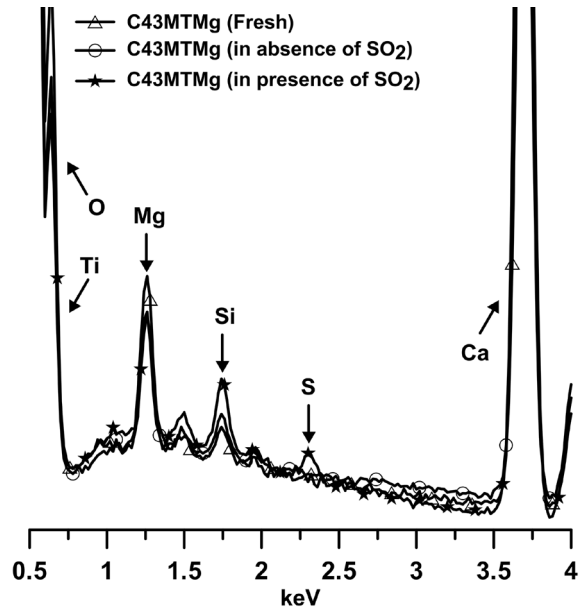


Figure 13 Partial EDX spectra of fresh C43MTMg, and particles subject to reactivity test in absence and presence of SO₂.

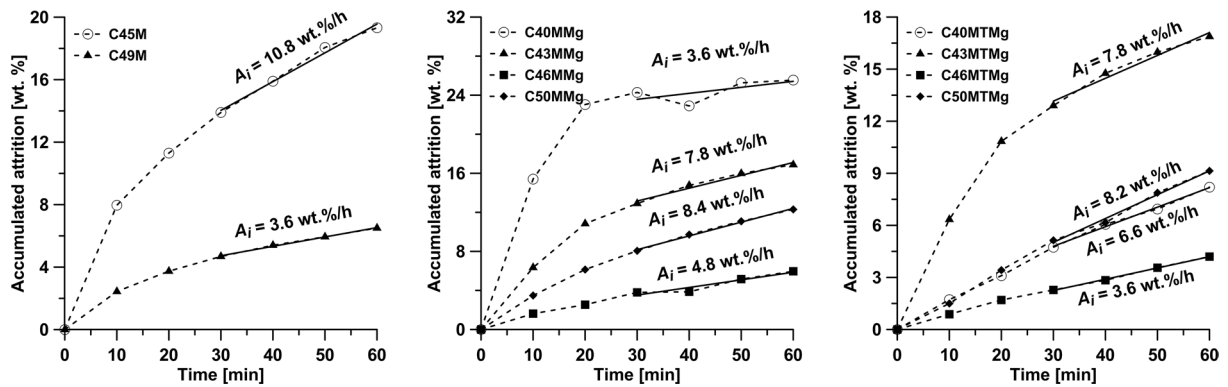


Figure 14 Accumulated attrition as a function of time for all investigated oxygen carriers. Note: For reasons of clarity, the scale of accumulated attrition is different in the figures.